buildings

MDPI

Article

Compatibility and Performance Evaluation of Early-Strength Admixtures in Repair Mortar Containing Recycled Concrete Powder and GGBFS

Yuanxin Guo [1], Wenna Li [1], Yepeng Wang [1], Gongbing Yue [1], Liang Wang [1,*], Xingang Xu [2], Qiuyi Li [1,*] and Mingxu Chen [1]

[1] College of Civil Engineering & Architecture, Qingdao Agricultural University, Qingdao 266109, China; 201901012@qau.edu.cn (Y.G.)
[2] State Key Laboratory of Silicate Materials for Architectures, Wuhan University of Technology, Wuhan 430070, China
* Correspondence: liangwang2019@qau.edu.cn (L.W.); 201801001@qau.edu.cn (Q.L.)

Abstract

Repair mortars containing recycled concrete powder (RCP) and ground granulated blast-furnace slag (GGBFS) are promising low-carbon materials for the rapid repair of concrete structures and pavements. However, their practical use is often limited by slow early hydration, insufficient early strength, and weak bonding with existing concrete substrates. In this study, four early-strength admixtures, namely calcium formate, anhydrous sodium sulfate, calcium acetate, and triethanolamine, were incorporated into a P·I 42.5 cement-based repair mortar containing RCP and a low dosage of GGBFS. Their effects on fluidity, flexural and compressive strength, tensile bond strength, drying shrinkage, and hydration characteristics were investigated. The results showed that the suitable dosages of calcium formate, anhydrous sodium sulfate, calcium acetate, and triethanolamine were 1.5%, 1.0%, 0.8%, and 0.05% by mass of total cementitious materials, respectively. Among the four admixtures, calcium formate provided the best balance among strength enhancement, bond performance, workability retention, and dosage tolerance. Compared with the control group, the 3 d and 28 d flexural strengths of the 1.5% calcium formate group increased by 37.0% and 20.3%, respectively. Anhydrous sodium sulfate gave the highest tensile bond strength, with the 14 d value increasing by 33.15% to 1.052 MPa, but its effective dosage range was relatively narrow. Calcium acetate was more effective in reducing drying shrinkage, with a 28 d shrinkage value of 695.14 $\times$ 10^{-6}. SEM and XRD results suggested that the admixtures mainly accelerated early hydration, while no new major crystalline phases were detected. Excessive dosages caused strength loss, bond deterioration, or increased drying shrinkage. These findings are applicable to the specific RCP–GGBFS repair mortar formulation and dosage ranges investigated here. They provide a practical basis for selecting early-strength admixtures for RCP-containing repair mortars used in concrete structure and pavement repair.

Keywords: recycled concrete powder; repair mortar; early-strength admixture; mechanical strength; tensile bond strength; drying shrinkage; microstructure

Check for updates

Academic Editor: Antonio Caggiano

Received: 13 May 2026
Revised: 8 June 2026
Accepted: 15 June 2026
Published: 17 June 2026

Copyright: © 2026 by the authors. Licensee MDPI, Basel, Switzerland. This article is an open access article distributed under the terms and conditions of the Creative Commons Attribution (CC BY) license.

1. Introduction

Carbon peaking and carbon neutrality have become important drivers for reducing carbon emissions in the construction industry. Under the requirements of the "14th Five-Year

Plan for the Comprehensive Utilization of Bulk Solid Waste", the building materials industry is encouraged to reduce clinker consumption and promote the high-value utilization of solid wastes [1–4]. At the same time, many existing buildings and municipal roads in China have entered a period of large-scale repair and renovation, while traditional cement-based repair mortars still face problems such as high carbon emissions, poor deformation compatibility with old substrates, and interface cracking [5,6]. Using recycled concrete powder (RCP) and ground granulated blast-furnace slag (GGBFS) as partial cement replacements in repair mortar provides a feasible way to reduce cement consumption and improve solid-waste utilization. In this study, the P·I 42.5 cement-based repair mortar containing RCP and a low dosage of GGBFS is hereafter referred to as RCP–GGBFS repair mortar. Previous studies have demonstrated the potential of recycled powder, slag-containing binders, and solid-waste-based cementitious materials in repair materials, pavement base stabilization, and other road engineering applications [7–11]. However, the early-age response of RCP–GGBFS repair mortar under rapid repair conditions remains insufficiently clarified. Kaptan et al. [12] reviewed the use of recycled concrete powder as a partial cement replacement and summarized its properties and activation methods, while Song et al. [13] reported the synergistic effect between recycled concrete powder and GGBFS in ternary blended cementitious systems. Vaičiukynienė et al. [14] further emphasized that sustainable repair mortars should meet the strict requirements of rapid rehabilitation of aging reinforced concrete structures. These studies provide a basis for using RCP and GGBFS in repair materials, but further discussion of GGBFS in different concrete systems is still needed.

GGBFS has been widely used in cementitious materials owing to its latent hydraulic activity and potential to reduce clinker consumption. Recent studies have investigated its application in pavement, heavy-duty, and structural concretes, focusing on workability, mechanical performance, shrinkage, abrasion resistance, durability, and carbon-emission reduction [15–18]. GGBFS has also been used in lightweight geopolymer concrete, recycled aggregate geopolymer concrete, and recycled concrete powder-based geopolymer systems, where it can contribute to strength development, pore refinement, and improved durability under suitable activation conditions [19–26]. These studies help define the broader role of GGBFS, but their conclusions are not directly applicable to the present low-GGBFS, RCP-containing repair mortar. For the present repair mortar containing RCP and a low dosage of GGBFS, the key issue is not the dosage effect of GGBFS itself but how chemical early-strength admixtures regulate early hydration, strength development, interfacial bonding, and volume stability.

Early-strength admixtures are often used when cementitious repair materials must gain strength rapidly without sacrificing workability or dimensional stability. Their effects are strongly dependent on admixture type, dosage, and binder composition. Previous studies have investigated several commonly used early-strength admixtures in ordinary cement-based or single solid-waste systems. Wang et al. [27] reported that calcium formate improved strength development and promoted hydration in cement composites containing fly ash and slag. Lyu et al. [28] analyzed the effects of calcium acetate on cement hydration, mechanical properties, and microstructure. He et al. [29] found that triethanolamine could affect the hydration kinetics of a cement–fly ash system and preferentially promote aluminate hydration under specific curing conditions. Other studies have also discussed the dosage ranges, synergistic effects, and low-carbon benefits of early-strength admixtures in cementitious or repair materials [30–34].

Although early-strength admixtures have been widely used in ordinary cement-based systems, their compatibility with RCP–GGBFS repair mortars remains unclear. Existing studies have mainly improved delayed hydration and slow strength development in solid waste-based cementitious systems through physical refinement or activation meth-

ods [35–37], while systematic comparison, compatibility optimization, and microstructural mechanism analysis of different early-strength admixtures are still insufficient. From a mechanistic perspective, the low early reactivity of RCP is closely related to its high SiO_2 content and relatively low CaO content. This composition indicates that RCP can provide siliceous surfaces but only limited readily soluble Ca-bearing species for early C-(A)-S-H formation. Therefore, the effect of early-strength additives in this system is expected to depend on how they regulate the early ionic environment and hydration products. Calcium formate and calcium acetate, as calcium carboxylate salts, may mainly improve early hydration by modifying the early reaction environment and promoting the precipitation of C-(A)-S-H/AFt-related hydration products [27,28,38]. Sodium sulfate may enhance the hydration of the cement–GGBFS fraction through sulfate activation and sulfate–aluminate reactions, including AFt formation [39]. Triethanolamine may mainly influence aluminate/ferrite reactions through complexation with Al-, Fe-, and Ca-bearing species, while its effect on silicate hydration is dose-dependent [38,40]. Based on this hypothesis, the present study compares calcium formate, calcium acetate, anhydrous sodium sulfate, and triethanolamine to clarify their compatibility with RCP–GGBFS repair mortar.

In this system, the key challenge is to improve early hydration and strength development without sacrificing workability, bond performance, or volume stability. Although formate-, sulfate-, acetate-, and alkanolamine-based additives have been widely used in cement-based materials, their compatibility and dosage sensitivity in repair mortar containing high-SiO_2 RCP and GGBFS remain insufficiently understood. In particular, the suitable dosage windows and possible overdosage effects of these additives have not been clearly established. Therefore, the objective of this study is to clarify the performance-regulating effects and suitable dosage ranges of calcium formate, anhydrous sodium sulfate, calcium acetate, and triethanolamine in the P·I 42.5 cement-based repair mortar containing RCP and a low dosage of GGBFS. To achieve this objective, fluidity, mechanical strength, tensile bond strength, and drying shrinkage were evaluated, and the performance differences were further interpreted using SEM and XRD. The results are expected to support the design of low-carbon repair mortars with improved early performance for concrete structure and pavement repair while promoting the resource utilization of recycled concrete powder.

2. Experimental Procedures

2.1. Experimental Materials

P·I 42.5 Portland cement (P·I 42.5), S95-grade ground granulated blast-furnace slag (GGBFS), and recycled concrete powder (RCP) were used as the main inorganic binders in this study. The cement was supplied by Fushun Cement Co., Ltd. (Fushun, China), and met the requirements of GB 175-2023 Common Portland Cement [41]. The S95-grade GGBFS was provided by Shandong Junhong Environmental Protection Technology Co., Ltd. (Zibo, China), with a 28-day activity index higher than 95%, in accordance with GB/T 18046-2017 Ground Granulated Blast Furnace Slag for Cement, Mortar, and Concrete [42]. The RCP was obtained from Qingdao Lvfan Renewable Resources Co., Ltd. (Qingdao, China). Its particle size was mainly distributed between 10 and 75 μm, and its properties satisfied the requirements of JG/T 573-2020 Recycled Fine Powder for Concrete and Mortar. The recycled fine aggregate (RFA) [43], also referred to as recycled sand, was obtained from Qingdao Lvfan Renewable Resources Co., Ltd. (Qingdao, China). Before use, the aggregate was washed to remove surface dust and impurities, naturally dried under ambient conditions, and then sieved. The RFA was used in an air-dried condition rather than in a saturated surface-dry condition. Particles smaller than 4.75 mm were selected as RFA for the preparation of repair mortar. Its properties complied with GB/T 25176-2010 Recycled Fine Aggregates for Concrete and Mortar [44]. Ethylene–vinyl acetate

redispersible polymer powder (RDP), supplied by Oulesi (Tianjin) Chemical Co., Ltd. (Tianjin, China), was used as the polymer modifier, while 6 mm recycled corn fiber (RCF), supplied by Hubei Xianyuan New Materials Co., Ltd. (Wuhan, China), was incorporated as the reinforcing fiber. A polycarboxylate ether superplasticizer (PCE) with a water-reduction rate of 30%, supplied by Beijing Kaili Tianwei Science and Trade Co., Ltd. (Beijing, China), was used to adjust the workability of the mixtures. Four early-strength admixtures, namely calcium formate (CF), anhydrous sodium sulfate (ASS), calcium acetate (CA), and triethanolamine (TEA), were selected to regulate the early performance of the repair mortar. Calcium formate was an industrial-grade white powder with an active content of at least 98%. Anhydrous sodium sulfate and calcium acetate were analytical-grade white powders with active contents higher than 99%, while triethanolamine was an analytical-grade colorless viscous liquid with an active content higher than 99%. CF, ASS, CA, and TEA were supplied by Shanghai Zengye Industrial Co., Ltd. (Shanghai, China), Sinopharm Chemical Reagent Co., Ltd. (Shanghai, China), Xi'an Tianmao Baoding Biotechnology Co., Ltd. (Xi'an, China), and JIAHUA Chemicals Inc. (Shanghai, China), respectively. The chemical compositions of the main raw materials are listed in Table 1.

Table 1. Chemical composition of P·I 42.5, GGBFS, and RCP (wt.%).

Material	SiO_2	Al_2O_3	CaO	Fe_2O_3	SO_3	Na_2O	MgO	Other
P·I 42.5	20.6	5.1	62.7	3.6	2.8	0.6	2.2	2.4
GGBFS	26.2	13.9	43.2	0.3	0.6	0.4	9.7	5.7
RCP	57.9	15.2	13.4	4.7	0.8	3.1	2.2	2.7

2.2. Experimental Design

Repair mortar containing recycled concrete powder and ground granulated blast-furnace slag, hereafter referred to as RCP–GGBFS repair mortar, was designed according to JC/T 2381-2016 Repair Mortar [45] and GB/T 25181-2019 Ready-mixed Mortar [46]. Following the conventional design of polymer-modified repair mortars, RDP was included as part of the total cementitious materials. The binder-to-aggregate ratio, water-to-binder ratio, PCE dosage, and RCF dosage were fixed at 1:1.5, 0.47, 1.0%, and 0.1% of the total mass of cementitious materials, respectively.

P·I 42.5 cement, RCP, GGBFS, and RDP were used as the cementitious components, and RFA was used as the fine aggregate. Four early-strength admixtures, namely calcium formate (CF), anhydrous sodium sulfate (ASS), calcium acetate (CA), and triethanolamine (TEA), were selected to regulate the performance of the RCP–GGBFS repair mortar. RCF and PCE were fixed in all mixtures so that the observed differences could be mainly attributed to the type and dosage of the early-strength admixture. RCF was fixed at 0.1% to provide a consistent fiber-bridging component. The PCE dosage was fixed at 1.0% for all mixtures to avoid the additional influence of varying superplasticizer content and to isolate the effects of early-strength additive type and dosage. During mixing, flowability testing, and casting, no visible segregation or bleeding was observed within the tested dosage ranges, including the CA-0.6% mixture with the highest flow value of 185 mm. Mixture uniformity was ensured by using the same mixing sequence, mixing time, casting procedure, and compaction method for all groups. In addition, the fresh mortar was cast immediately after the flowability test to reduce possible changes in consistency before molding.

The dosage gradients of the four early-strength additives are shown in Table 2, and the detailed mix proportions are listed in Table 3. The dosage ranges were selected according to the commonly reported dosage levels of similar additives in cement-based materials and were further adjusted through preliminary trial tests for the present RCP–GGBFS repair mortar. Dosages causing severe fluidity loss, abnormal setting, or obvious strength

reduction were excluded. Different dosage ranges were adopted because the four additives have different chemical activities and effective dosage windows. CF and CA were selected in moderate dosage ranges as calcium carboxylate salts, while ASS was tested at around 1.0%, considering the possible adverse effect of excessive sulfate, and TEA was used at a much lower dosage because of its high activity and dosage sensitivity. The suitable dosage of each additive was determined from the combined performance in fluidity, mechanical strength, tensile bond strength, and drying shrinkage.

Table 2. Different dosages of early strength admixtures for the four groups.

Group	1	2	3	4
Calcium formate	0.5%	1%	1.5%	2%
Anhydrous sodium sulfate	0.8%	1.0%	1.2%	1.4%
Calcium acetate	0.4%	0.6%	0.8%	1.0%
Triethanolamine	0.01%	0.03%	0.05%	0.07%

Note: The dosage of the early-strength agent is (wt.%) of the total mass of the cementitious materials.

Table 3. Design of test mix proportions for RCP–GGBFS repair mortar.

Group	P·I 42.5/g	RCP/g	GGBFS/g	RDP/g	RFA/g	PCE/g	RCF/g	ES/g	Water/g
Control group	734.4	43.2	17.28	69.12	1296.0	8.64	0.86	0	406
CF 1	734.4	43.2	17.28	69.12	1296.0	8.64	0.86	4.32	406
CF 2	734.4	43.2	17.28	69.12	1296.0	8.64	0.86	8.64	406
CF 3	734.4	43.2	17.28	69.12	1296.0	8.64	0.86	12.96	406
CF 4	734.4	43.2	17.28	69.12	1296.0	8.64	0.86	17.28	406
ASS 1	734.4	43.2	17.28	69.12	1296.0	8.64	0.86	6.91	406
ASS 2	734.4	43.2	17.28	69.12	1296.0	8.64	0.86	8.64	406
ASS 3	734.4	43.2	17.28	69.12	1296.0	8.64	0.86	10.37	406
ASS 4	734.4	43.2	17.28	69.12	1296.0	8.64	0.86	12.10	406
CA 1	734.4	43.2	17.28	69.12	1296.0	8.64	0.86	3.46	406
CA 2	734.4	43.2	17.28	69.12	1296.0	8.64	0.86	5.18	406
CA 3	734.4	43.2	17.28	69.12	1296.0	8.64	0.86	6.91	406
CA 4	734.4	43.2	17.28	69.12	1296.0	8.64	0.86	8.64	406
TEA 1	734.4	43.2	17.28	69.12	1296.0	8.64	0.86	0.86	406
TEA 2	734.4	43.2	17.28	69.12	1296.0	8.64	0.86	2.59	406
TEA 3	734.4	43.2	17.28	69.12	1296.0	8.64	0.86	4.32	406
TEA 4	734.4	43.2	17.28	69.12	1296.0	8.64	0.86	6.05	406

Note: CF = calcium formate; ASS = anhydrous sodium sulfate; CA = calcium acetate; TEA = triethanolamine; RCP = recycled concrete powder; GGBFS = ground granulated blast-furnace slag; RDP = redispersible polymer powder; RFA = recycled fine aggregate; PCE = polycarboxylate ether superplasticizer; RCF = recycled corn fiber. The dosage of early-strength admixtures is expressed as the mass percentage of total cementitious materials. The mixing water dosage reported in the mix proportion refers to the added mixing water, and the RFA was used in an air-dried condition.

2.3. Test Methods

2.3.1. Sample Preparation Process

All raw materials were weighed according to the designed mix proportions. P·I 42.5 cement, RCP, GGBFS, RDP, RCF, PCE, and RFA were first added to a cement mortar mixer (JJ-5, Zhejiang Tugong Instrument Manufacturing Co., Ltd., Shaoxing, China) and dry-mixed at low speed to improve the dispersion of powders, fibers, and aggregate. The mixing water was then added together with the corresponding early-strength additive, and mixing was continued until a homogeneous fresh mortar was obtained. For TEA, the liquid additive was premixed with water before being introduced into the dry materials. After mixing, the fluidity of the fresh mortar was measured immediately. The mortar was then cast into 40 mm × 40 mm × 160 mm steel molds in two layers. The same casting and compaction procedure was used for all mixtures. A vertical load of 50 kN was applied

and maintained for 60 s to compact the specimens. The molded specimens were covered with plastic film for 24 h to prevent moisture loss. After demolding, the specimens were transferred to a standard curing chamber at 20 ± 2 °C and relative humidity ≥ 95% until the specified testing age. During specimen preparation, no visible segregation or bleeding was observed in any mixture, including the CA mixture with the highest flow value. The same mixing, casting, and compaction procedures were adopted for all mixtures to reduce preparation-induced variation.

To make the experimental program clearer, the test design was divided into three parts: preparation of the reference RCP–GGBFS repair mortar, single-factor dosage optimization of four early-strength admixtures, and performance evaluation of the optimized mixtures. A total of 17 mixtures were prepared, including one control mixture and 16 mixtures containing one of the four early-strength admixtures at four dosage levels. The binder-to-aggregate ratio, water-to-binder ratio, RDP dosage, PCE dosage, and RCF dosage were kept constant. The varied factors were the type and dosage of the early-strength additive. The measured parameters included fluidity, flexural strength, compressive strength, tensile bond strength, drying shrinkage, SEM morphology, and XRD phase composition. The overall experimental design and specimen preparation procedure are shown in Figure 1.

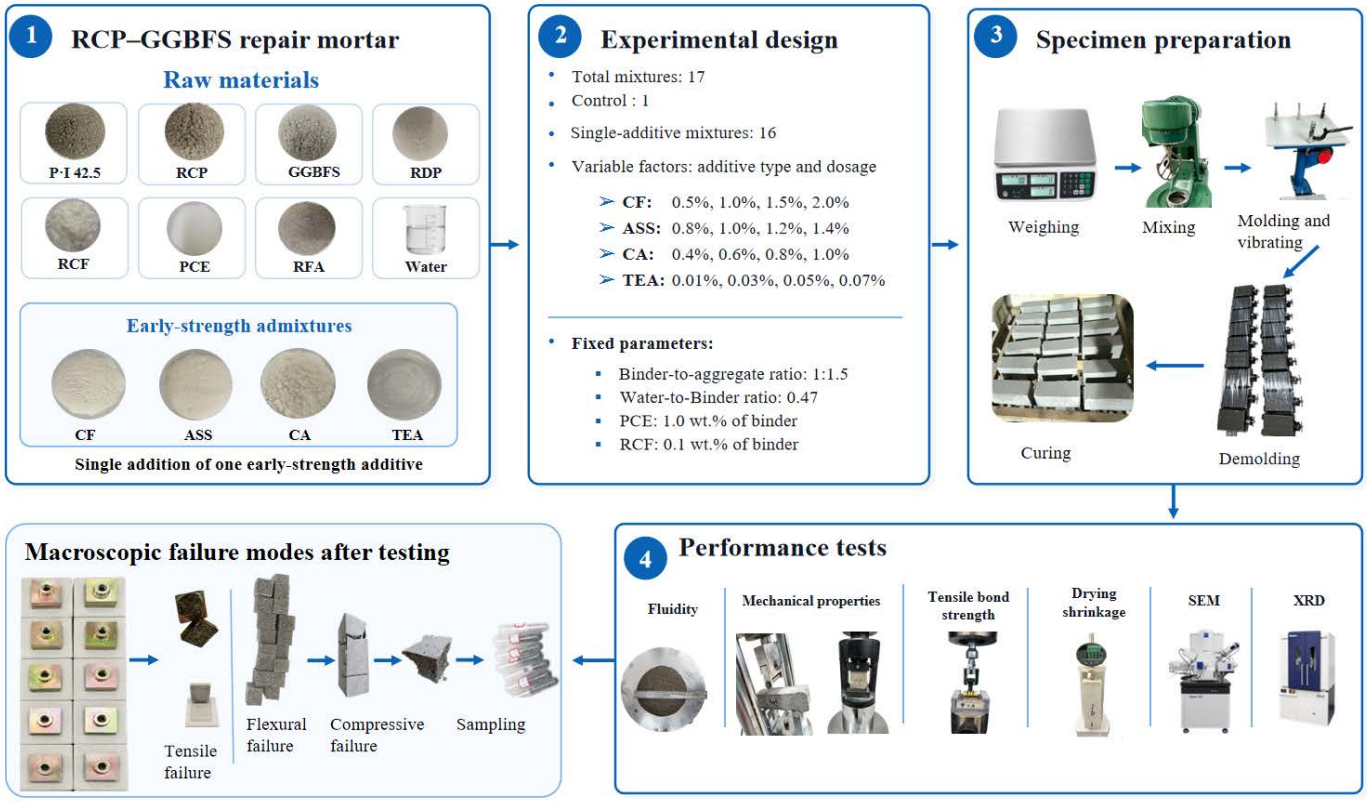


Figure 1. Experimental flowchart for the preparation and testing of RCP–GGBFS repair mortar.

2.3.2. Fluidity Test

The RCP–GGBFS repair mortar fluidity test strictly complies with the GB/T 2419-2005 standard, "Test Method for Fluidity of Cement Mortar" [47]. The test environment is maintained at a temperature of 20 ± 2 °C and a relative humidity of ≥50%. Upon completion of the jolting, the diameters of the bottom surface of the cement mortar were measured in two mutually perpendicular directions using a vernier caliper. The average value was calculated and rounded to the nearest integer (unit: mm), and this average value is defined as the cement mortar fluidity at the corresponding water content.

2.3.3. Mechanical Property Test

Mechanical property testing of RCP–GGBFS repair mortar was conducted in accordance with GB/T 17671-2021, "Test Methods for the Strength of Cement Mortar (ISO Method)"[48]. The flexural and compressive strengths of the test specimens were measured at 3 d, 7 d, and 28 d of curing, with three parallel specimens tested in each group, and the results were averaged.

2.3.4. Tensile Bond Strength Test

Tensile bond strength was evaluated according to the 14 d requirement specified in JC/T 2381-2016 "Repair Mortar", and the test procedure was conducted with reference to JGJ/T 70-2009 "Standard for Test Method of Basic Properties of Construction Mortar"[49]. After curing the specimens for 13 d under standard conditions, a high-strength epoxy adhesive supplied by Wenzhou Anergu New Materials Co., Ltd. (Wenzhou, China) was applied to the specimen surfaces. The tensile fixtures were aligned and affixed to the specimens, followed by an additional 24 h of curing. Tensile tests were conducted using a universal testing machine (WDW-200D, Changchun New Testing Machine Co., Ltd., Changchun, China) at a loading rate of 5 ± 1 mm/min, and the failure load of the specimens was recorded. No 3 d or 7 d tensile bond strength tests were conducted in this study; therefore, the bond strength results reflect the standard-age bonding performance rather than the very early development of interfacial bond strength.

2.3.5. Testing of Drying Shrinkage Properties

The drying shrinkage performance test was conducted in accordance with JC/T 2381-2016 "Repair Mortar". The drying shrinkage values of the test specimens were measured at ages of 3, 7, 14, 21, and 28 d. Each test group consisted of three parallel specimens, and the results were averaged.

2.3.6. Microscopic Performance Testing

For microstructural testing, mortar specimens from the control group and the mixtures with the optimal dosages of the four early-strength admixtures were selected at 3 d and 28 d. Hydration was stopped using anhydrous ethanol, supplied by Yantai Sanhe Chemical Reagent Co., Ltd. (Yantai, China). For SEM observation, fresh fractured fragments were collected from the inner part of the specimens. SEM observations were performed using a ZEISS Sigma 360 scanning electron microscope (Carl Zeiss Microscopy GmbH, Oberkochen, Germany). The SEM images were used to qualitatively observe the local morphology of hydration products and selected interfacial regions. For XRD analysis, powder samples were collected from the inner part of the hardened mortar specimens. Matrix-rich fragments from different positions were selected, and visible recycled aggregate particles were removed as far as possible to reduce the influence of quartz-bearing aggregate. XRD analysis was conducted using a Rigaku Ultima IV X-ray diffractometer (Rigaku Corporation, Tokyo, Japan). However, because recycled fine aggregate contains attached old mortar and RCP also contains residual quartz-bearing particles, the influence of residual quartz could not be completely eliminated. The selected fragments were dried, ground, passed through a 75 μm sieve, and homogenized before testing. The XRD scan range was 10°–80° 2θ. It should be noted that the strongest AFt reflection near 9° 2θ was not included in this scan range. Therefore, the XRD results were used mainly for qualitative phase identification rather than quantitative comparison of phase contents or hydration degree.

2.3.7. Statistical Analysis

All results are presented as mean ± standard deviation from independent repeated measurements. Three parallel specimens were tested for flexural strength, compressive strength, and drying shrinkage. For tensile bond strength, ten specimens were prepared per mixture; invalid results were excluded per JGJ/T 70-2009, with a minimum of six valid values retained for statistical calculation. Statistical comparisons were performed using Welch's *t*-tests for flexural strength, compressive strength, and drying shrinkage between modified mixtures and the control group. For tensile bond strength, one-way ANOVA followed by Dunnett's post hoc test was used for comparisons with the control group, with a separate comparison between ASS-1.4% and ASS-1.0% to evaluate excessive dosage effects. Significance levels were set at ** ($p < 0.01$), and *** ($p < 0.001$). Flowability and compressive-to-flexural strength ratio were not statistically analyzed, as they were derived from single tests or mean values, respectively. Statistical analyses and plotting were performed using OriginPro 2026 (OriginLab Corporation, Northampton, MA, USA).

3. Results and Discussion

3.1. Fluidity of RCP–GGBFS Repair Mortar

Figure 2 shows the fluidity of RCP–GGBFS repair mortar with different types and dosages of early-strength admixtures. The control mixture had a flow value of 178 mm. The CF mixtures showed relatively stable flow values, ranging from 177 to 181 mm, indicating that calcium formate had little adverse effect on workability within the tested dosage range. The ASS mixtures showed a more obvious dosage-dependent decrease in fluidity. The flow value was 178 mm at 1.0% ASS, which was close to the control mixture, but decreased to 168 mm when the dosage increased to 1.4%. This decrease may be related to the reduced dispersion efficiency of the PCE-based system in the presence of excessive sulfate ions. Similar effects of sulfate ions on the adsorption and dispersing performance of polycarboxylate superplasticizers have been reported in previous studies [50,51]. For CA, the flow values ranged from 175 to 185 mm, with the highest value appearing at 0.6%. At the selected dosage of 0.8%, the flow value was 180 mm, still close to the control mixture. The TEA mixtures showed flow values between 174 and 181 mm, and the selected dosage of 0.05% gave a flow value of 181 mm. At the selected dosages, none of the four admixtures caused a clear loss of workability. CF and TEA had little influence on flowability, whereas CA slightly improved the flow value at moderate dosage, and excessive ASS caused the most evident reduction.

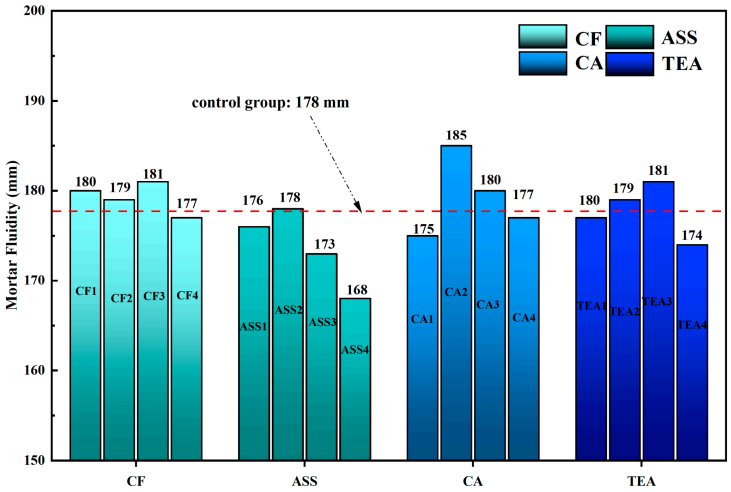


Figure 2. Flowability of RCP–GGBFS repair mortar with different types and dosages of early-strength admixtures. The values represent measured flowability results.

3.2. Mechanical Properties of RCP–GGBFS Repair Mortar

The effects of different types and dosages of early-strength admixtures on the flexural and compressive strengths of RCP–GGBFS repair mortar are shown in Figures 3 and 4. For each mixture, both flexural and compressive strengths generally increased with curing age. The comparison among the tested dosage levels shows that the four admixtures exhibited similar dosage-dependent responses: the strengths increased at moderate dosages but decreased when the dosage exceeded the suitable range. This indicates that the strength development depended not only on the admixture type but also on whether the dosage was within its effective range.

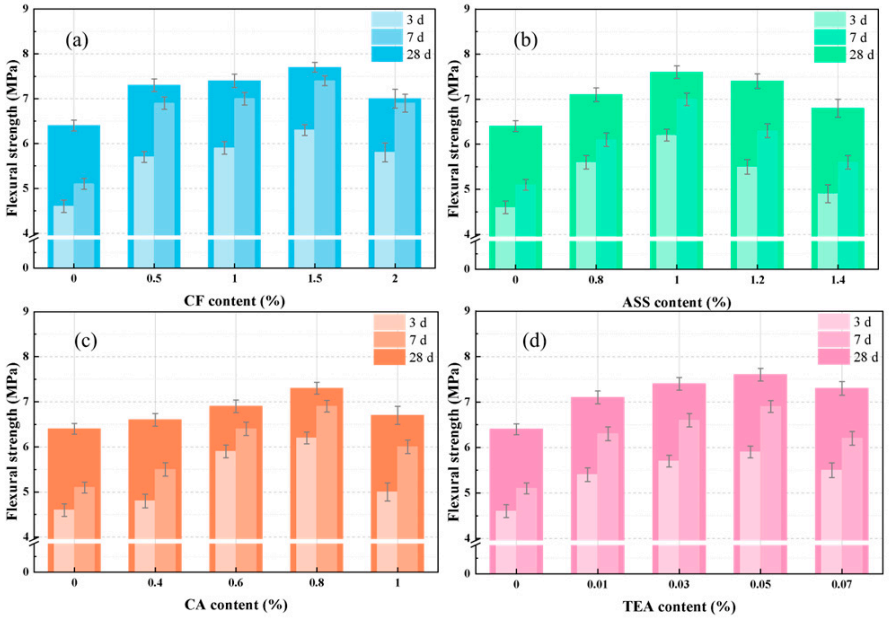


Figure 3. Flexural strength of RCP–GGBFS repair mortar with different types and dosages of early-strength admixtures. Error bars represent standard deviation: (**a**) CF; (**b**) ASS; (**c**) CA; (**d**) TEA.

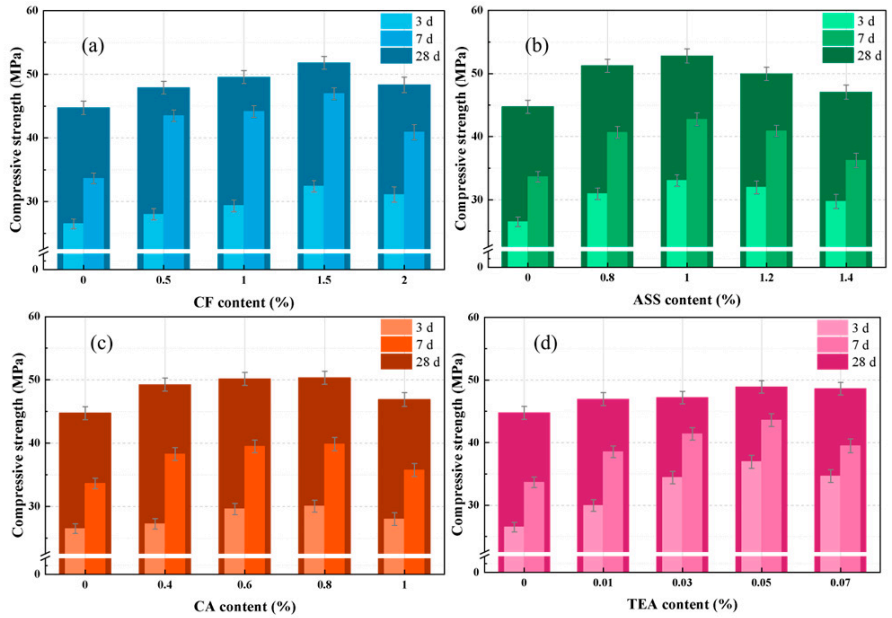


Figure 4. Compressive strength of RCP–GGBFS repair mortar with different types and dosages of early-strength admixtures. Error bars represent standard deviation: (**a**) CF; (**b**) ASS; (**c**) CA; (**d**) TEA.

Based on the strength results, the suitable dosages of CF, ASS, CA, and TEA were determined as 1.5%, 1.0%, 0.8%, and 0.05% of the total mass of cementitious materials, respectively. At these dosages, both flexural and compressive strengths were higher than those of the control group. TEA showed the most obvious improvement in early compressive strength, with the 3 d compressive strength increasing by 39.4% compared with the control group. ASS contributed most to the 28 d compressive strength, with an increase of 18.0%. For flexural strength, the CF mixture showed increases of 37.0% at 3 d and 20.3% at 28 d. Overall, the beneficial effect of each admixture was dosage-limited: moderate additions promoted strength development, whereas excessive additions weakened the improvement.

The 28 d compressive-to-flexural strength ratio was used to compare the relative balance between compressive and flexural performance. According to JC/T 2381-2016, the ratio of repair mortar should not exceed 7.0. As shown in Figure 5, the control group reached 6.99, close to the specified limit. All mixtures with the optimal dosages of early-strength admixtures showed lower ratios than the control group, indicating reduced apparent brittleness. Among the modified mixtures, TEA showed the lowest ratio, followed by CF, CA, and ASS. Combined with the absolute strength results in Figures 3 and 4, the decrease in the ratio was mainly associated with improved flexural performance, while the compressive strength was still maintained at an acceptable level. Therefore, the compressive-to-flexural strength ratio is discussed here as an apparent brittleness index rather than direct evidence of toughness improvement. This interpretation is also consistent with previous work on redispersible-polymer-powder-modified repair mortars, where polymer powders were found to affect compressive and flexural strengths differently depending on polymer type and dosage [52].

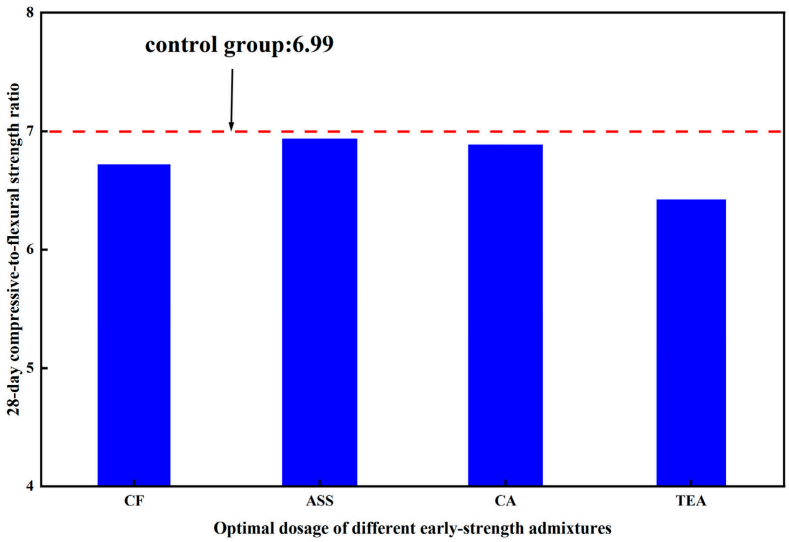


Figure 5. Compressive-to-flexural strength ratio at 28 d for RCP–GGBFS repair mortar with the optimal dosage of different early-strength admixtures. The ratio was calculated from the mean compressive and flexural strengths.

3.3. Tensile Bond Strength of RCP–GGBFS Repair Mortar

For repair mortars, tensile bond strength directly reflects whether the repair layer can remain attached to the existing concrete substrate. It is affected by the properties of the repair mortar, the condition of the substrate surface, and the compatibility between the repair layer and the substrate [5]. As shown in Figure 6, the 14 d tensile bond strength of the control group was 0.790 MPa, which was lower than the minimum requirement of JC/T

2381-2016. This indicates that the unmodified RCP-GGBFS repair mortar had insufficient bonding performance under the present mix proportion.

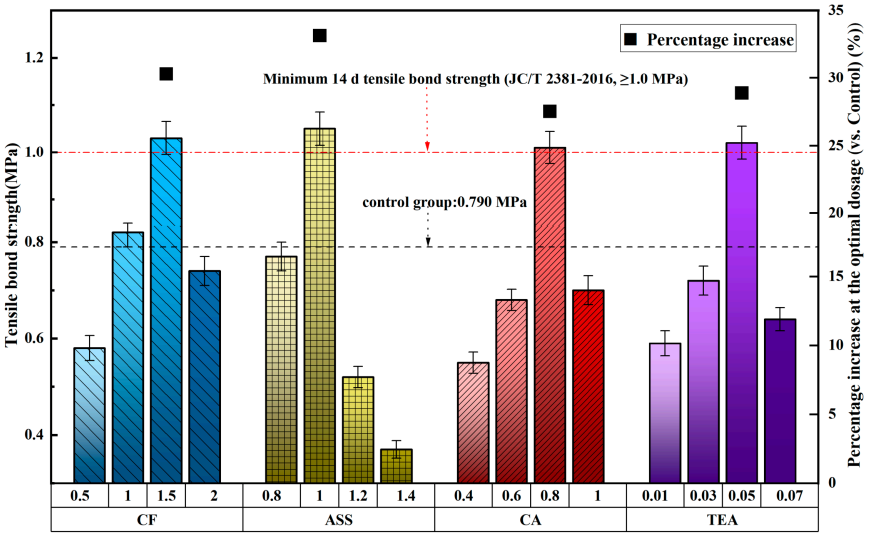


Figure 6. The effect of different types and dosages of early-strength admixtures on the 14 d tensile bond strength of RCP–GGBFS repair mortar.

All four early-strength admixtures improved the bond strength at suitable dosages, and the bond strength generally first increased and then decreased with increasing dosage. Among them, ASS showed the highest bond strength at 1.0%, reaching 1.052 MPa, which was 33.15% higher than that of the control group. When the ASS dosage increased to 1.4%, the tensile bond strength decreased sharply to 0.370 MPa, indicating that ASS had a narrow effective dosage range in this system. At a suitable dosage, sulfate ions may promote early hydration and improve the filling of hydration products near the repair–substrate interface. However, excessive sulfate may disturb the interfacial hydration balance and favor the local accumulation of sulfate-bearing hydration or crystallization products in weak interfacial regions. These products may generate crystallization pressure and promote microcrack development, thereby weakening the bond between the repair mortar and the substrate. Similar sulfate-related expansion and damage mechanisms have been associated with crystallization pressure in cementitious materials [53]. CF also showed a clear improvement in bonding performance. At 1.5%, the tensile bond strength increased by 30.30% compared with the control group, and the decrease at higher dosages was relatively limited, suggesting better dosage tolerance than ASS. CA and TEA showed weaker improvements than ASS and CF, but their optimal dosages still allowed the bond strength to meet the specification requirement. Overall, ASS provided the highest bond strength at the suitable dosage, whereas CF showed more stable bonding performance and better tolerance to dosage variation.

3.4. Drying Shrinkage Properties

Figure 7 shows the drying shrinkage of RCP–GGBFS repair mortar with different types and dosages of early-strength admixtures. The control mixture showed a relatively high 28 d drying shrinkage of 2572.38×10^{-6}. The relatively high drying shrinkage of the control mixture was likely related to the formulation characteristics, particularly the incorporation of recycled fine aggregate and RCP. The water-to-binder ratio of 0.47 reported in this study is the nominal ratio based on the added mixing water. Because the RFA was used in an air-dried condition rather than in a saturated, surface-dry condition, the adhered old mortar on the RFA may have absorbed part of the mixing water, thereby affecting the

effective water distribution and drying shrinkage behavior. In addition, RCP may increase water demand in the fresh mixture, while the low GGBFS content limited its possible pore-refining and shrinkage-reducing effect. Previous studies have shown that recycled fine aggregate can affect the effective water-to-cement ratio and drying shrinkage of mortar because of its water absorption and moisture transport characteristics [54].

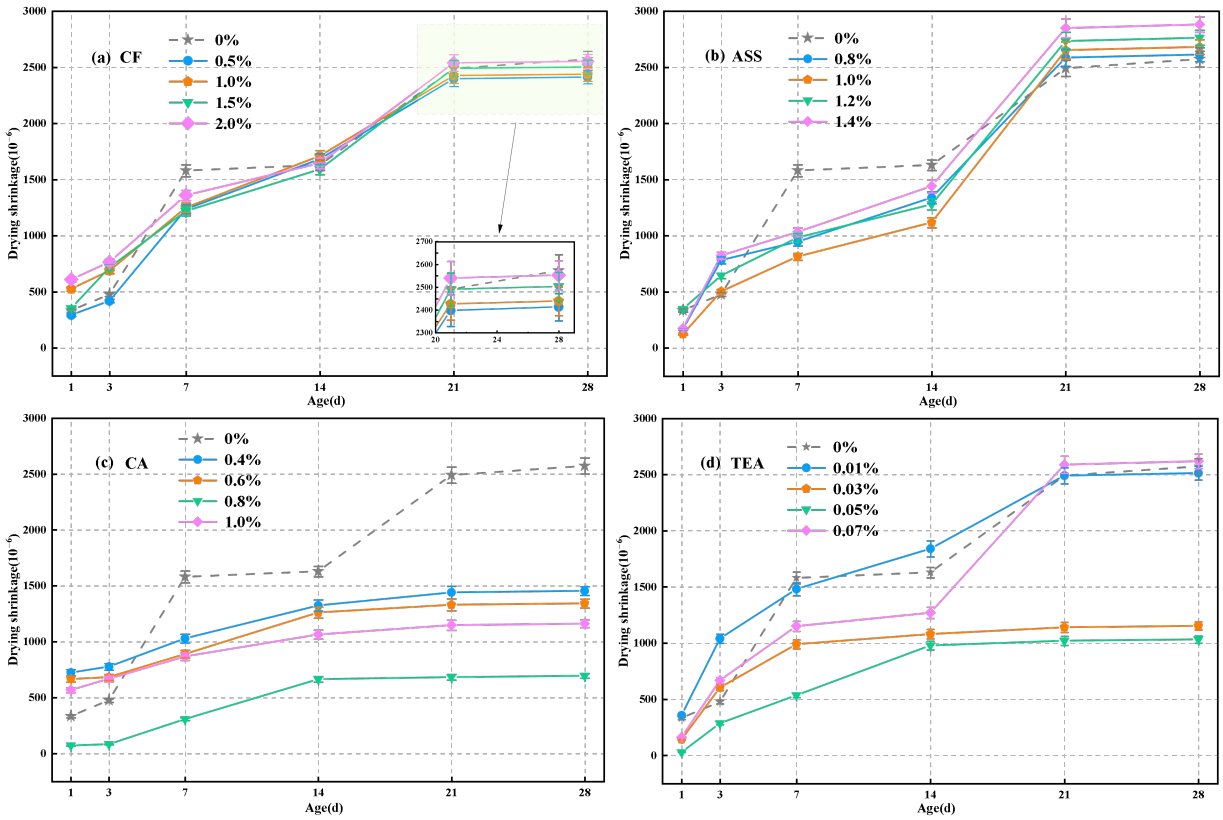


Figure 7. The effect of different types and dosages of early strength admixtures on the drying shrinkage of RCP–GGBFS repair mortar: (**a**) CF; (**b**) ASS; (**c**) CA; (**d**) TEA. Lines are used only to indicate the time-dependent development of drying shrinkage.

The four admixtures showed different effects on drying shrinkage. CF had only a limited influence, and the 28 d shrinkage values of the CF mixtures were close to that of the control group. ASS reduced shrinkage at early ages, especially at 0.8% and 1.0%, but the shrinkage increased rapidly after 14 d and became higher at later ages when the dosage was increased. This indicates that excessive sulfate addition may be unfavorable for volume stability. CA showed the most obvious shrinkage reduction in the present formulation. At 0.8%, the 28 d drying shrinkage decreased to 695.14 $\times$ 10^{-6}, which was much lower than that of the control group. This shrinkage reduction should be interpreted as a formulation-dependent result, rather than as a general shrinkage-reducing function of calcium acetate. A moderate CA dosage may promote more balanced hydration product formation and reduce connected capillary pores, thereby decreasing moisture migration during drying. TEA also reduced shrinkage at moderate dosages, with 0.05% showing the best effect, while the shrinkage increased again at 0.07%. Overall, CA was the most effective additive for shrinkage reduction in the present RCP–GGBFS repair mortar, whereas ASS should be carefully controlled when volume stability is considered.

3.5. Statistical Analysis of Key Macroscopic Properties

Table 4 summarizes the statistical comparisons used to verify the main performance differences. Only comparisons directly related to the main conclusions were included.

CF-1.5% significantly improved flexural strength at both 3 d and 28 d. TEA-0.05% increased the 3 d compressive strength, whereas ASS-1.0% increased the 28 d compressive strength. For tensile bond strength, ASS-1.0% and CF-1.5% were significantly higher than the control group, while ASS-1.4% was significantly lower than ASS-1.0%, confirming the narrow effective dosage range of ASS. CA-0.8% and TEA-0.05% significantly reduced the 28 d drying shrinkage. These statistical results are consistent with the macroscopic trends, but the final dosage selection was based on the combined performance in strength, bond strength, and drying shrinkage.

Table 4. Statistical significance of key comparisons between optimized mixtures and the control group.

Property	Age	Comparison	*p*-Value	Significance
Flexural strength	3 d	CF-1.5% vs. Control	$p < 0.001$	***
Flexural strength	28 d	CF-1.5% vs. Control	$p < 0.001$	***
Compressive strength	3 d	TEA-0.05% vs. Control	$p < 0.001$	***
Compressive strength	28 d	ASS-1.0% vs. Control	$p < 0.001$	***
Tensile bond strength	14 d	ASS-1.0% vs. Control	$p < 0.001$	***
Tensile bond strength	14 d	CF-1.5% vs. Control	$p < 0.001$	***
Tensile bond strength	14 d	ASS-1.4% vs. ASS-1.0%	$p < 0.001$	***
Drying shrinkage	28 d	CA-0.8% vs. Control	$p < 0.001$	***
Drying shrinkage	28 d	TEA-0.05% vs. Control	$p < 0.001$	***
Drying shrinkage	28 d	ASS-1.4% vs. Control	$p < 0.01$	**

Note: *p*-values for flexural strength, compressive strength, and drying shrinkage were obtained from pairwise Welch's *t*-tests. For tensile bond strength, *p*-values were obtained from one-way ANOVA followed by Dunnett's post hoc test. The comparison between ASS-1.4% and ASS-1.0% was conducted separately. Significance levels are defined as follows: **, $p < 0.01$; and ***, $p < 0.001$.

3.6. Microscopic Structure

In the SEM images, needle-like crystals, flocculent products, and plate-like crystals are assigned to AFt, C-S-H gel, and CH, respectively, according to the typical morphology of cement hydration products. These assignments are used for qualitative morphological discussion. In addition, the sample preparation and observation description in Section 2.3.6 has been clarified to state that fresh fractured fragments from the inner part of the specimens were used for SEM observation.

Figure 8 shows the SEM images of the control RCP–GGBFS repair mortar at 3 d and 28 d. At 3 d, only a small amount of AFt and C-S-H gel can be observed, and the hydration products are scattered around the particles. Some open pores, loose areas, and plate-like CH crystals are still visible, indicating that the early hydration of the control mixture was limited. At 28 d, more C-S-H gel and needle-like AFt-like hydration products appear in the matrix, and the local structure becomes more compact than that at 3 d. However, pores and unhydrated particles can still be observed, suggesting that hydration was still incomplete and that the matrix was not fully densified.

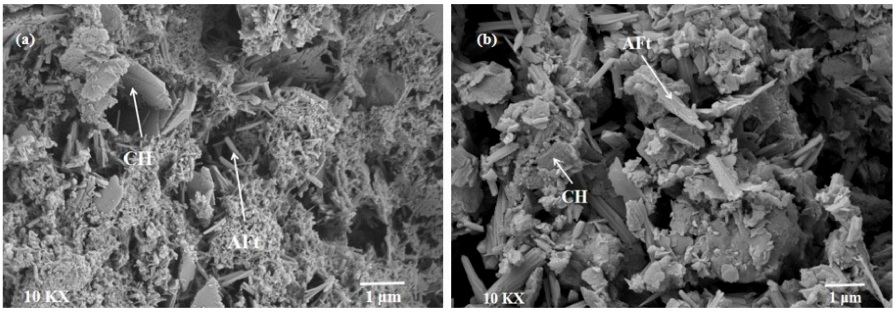


Figure 8. SEM images of the control group at 3 d and 28 d: (**a**) 3 d; (**b**) 28 d.

Figure 9 presents the 3 d SEM images of the mixtures containing the optimal dosages of different early-strength admixtures. Compared with the control mixture, more hydration products are observed in the modified mixtures. In the CF mixture, AFt crystals and C-S-H gel are locally intergrown around the particles, showing a more developed early hydration morphology. This is consistent with previous findings that calcium formate can promote early strength development and AFt formation in Portland cement–fly ash/slag blended systems [27]. In the ASS mixture, relatively long AFt-like hydration products are evident, which is related to the sulfate supplied by anhydrous sodium sulfate. Similar sulfate-induced acceleration of early-age strength has also been reported in blended cement systems containing high-volume fly ash [55]. C-S-H gel and CH crystals are also present, indicating the formation of mixed hydration products at the suitable ASS dosage. The CA mixture shows a relatively uniform distribution of AFt-like hydration products and C-S-H gel, while large CH crystals are less prominent. Previous work has shown that calcium acetate can affect the reaction process, strength development, and microstructure of cementitious materials, although its effect depends on the binder system [28]. This morphology suggests a more balanced development of early hydration products. Previous studies have reported that TEA can affect Portland cement hydration in a dosage-dependent manner, especially by influencing aluminate/ferrite-related phases such as C_3A and C_4AF, as well as calcium silicate phases such as C_3S and C_2S [56]. In the present RCP–GGBFS repair mortar, the silicate-related reactive phases mainly include C_3S/C_2S from Portland cement and the Ca–Si–Al glassy phase in GGBFS, while the aluminate/ferrite-related phases mainly include C_3A/C_4AF from Portland cement and Al-bearing glassy phases in GGBFS. The obvious CH crystals and the less continuous distribution of C-S-H gel in the observed TEA region suggest that the promotion of C-(A)-S-H formation was limited under the tested TEA dosage.

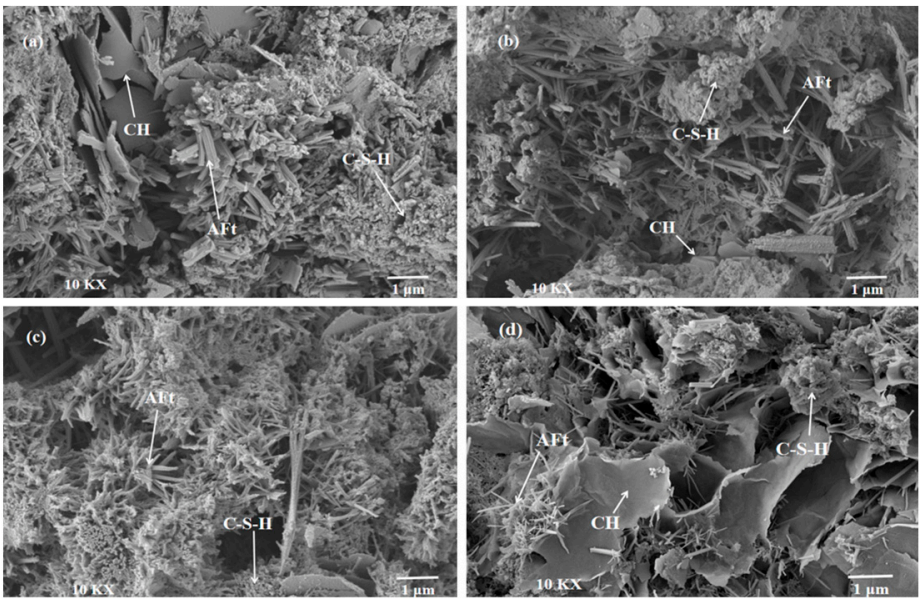


Figure 9. SEM of RCP–GGBFS repair mortar at 3 d at the optimal dosage of different early-strength admixtures: (**a**) CF; (**b**) ASS; (**c**) CA; (**d**) TEA.

Figure 10 shows the SEM images of the mixtures with the optimal dosages of different early-strength admixtures after 28 d curing. Compared with the 3 d samples, more hydration products were observed in the selected regions after 28 d curing. In the CF mixture, C-S-H gel was more widely distributed around the particles, and plate-like CH crystals were embedded in the surrounding hydration products. In the ASS mixture,

needle-like AFt-type products and C-S-H gel were still observed, but the sulfate-related products should be controlled because excessive ASS caused a sharp decrease in bond strength. In the CA mixture, AFt-type products and C-S-H gel appeared to be relatively continuous in the observed region, which may be related to the lower drying shrinkage of this group. In the TEA mixture, CH crystals remained obvious, and the distribution of C-S-H gel appeared less continuous than that in the CF and CA mixtures. Overall, the SEM observations indicate that the four admixtures affected hydration product formation to different extents, but these images should be regarded as local morphological evidence rather than quantitative proof of complete hydration or overall matrix density.

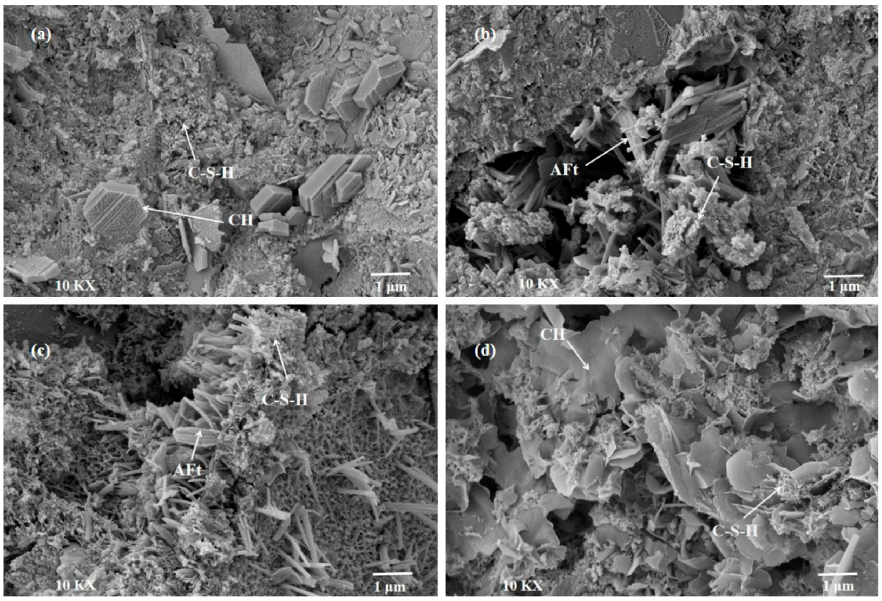


Figure 10. SEM of RCP–GGBFS repair mortar at 28 d at the optimal dosage of different early-strength admixtures: (**a**) CF; (**b**) ASS; (**c**) CA; (**d**) TEA.

Representative lower-magnification SEM images of selected fractured surfaces are provided in Figure 11 to show the general morphology of the observed regions. The high-magnification SEM images were used for qualitative comparison of local hydration products. It should be noted that the SEM observations were performed on fractured surfaces and were therefore used only as qualitative morphological evidence, rather than for quantitative porosity analysis.

Figure 12 shows the XRD patterns of the control mixture and the mixtures containing the optimal dosages of different early-strength admixtures at 3 d and 28 d. The main crystalline phases identified in all samples are quartz, calcite, portlandite, and residual calcium silicates, mainly C_3S and C_2S. No new dominant crystalline phases are detected, indicating that the early-strength admixtures mainly regulate hydration rather than change the main phase composition of the hardened mortar. Quartz is mainly introduced by recycled fine aggregate and recycled concrete powder. Because residual quartz-bearing particles may influence the quartz peak intensity, this peak is not used for quantitative comparison among mixtures. The calcite peaks observed in the XRD patterns are mainly attributed to carbonate phases introduced by the recycled constituents, especially RCP and RFA. Since these materials were derived from waste concrete, they may contain carbonated old cement paste, carbonate-containing aggregate particles, or other carbonate phases before mixing. Therefore, the $CaCO_3$ peaks should not be directly interpreted as evidence of significant carbonation during curing. At 3 d, the changes in portlandite and residual clinker-related peaks suggest that the admixtures affected early hydration to different degrees. At 28 d, the differences among mixtures become smaller, showing further

hydration development with curing age. This agrees with the macroscopic results, where the admixtures mainly improve early-age performance. AFt was not clearly identified in the XRD patterns. This is mainly because the strongest AFt reflection near 9° 2θ was outside the scanned range of 10°–80° 2θ, while the remaining reflections were weak or partly overlapped with other crystalline phases. Therefore, the absence of a clear AFt peak does not exclude AFt formation. The needle-like products observed in SEM were tentatively regarded as AFt-like hydration products based on their typical morphology. A broad diffuse region in the range of approximately 25°–35° may be associated with poorly crystalline C-S-H/C-A-S-H gels. However, this region overlaps with the reflections of quartz, calcite, portlandite, and residual calcium silicates. Therefore, the shaded region is used only to indicate the possible contribution of gel-like hydration products rather than a well-defined crystalline phase. Overall, the SEM and XRD results are complementary, suggesting that the admixtures promoted hydration product formation to different extents without producing new dominant crystalline phases.

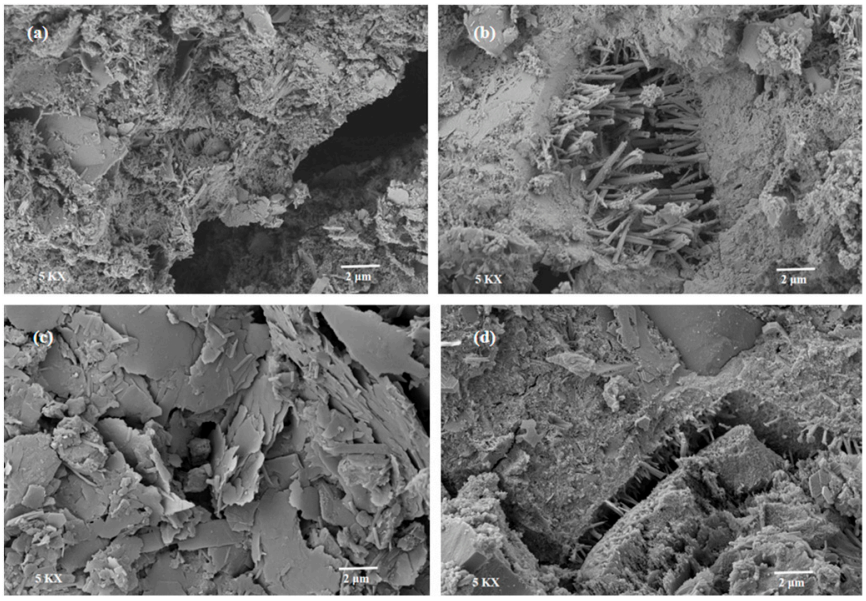


Figure 11. Representative lower-magnification SEM images of selected fractured surfaces: (**a**) Control, 3 d; (**b**) CF, 3 d; (**c**) Control, 28 d; (**d**) CF, 28 d. These images show the general morphology of selected fractured regions, while the 10,000× SEM images in Figures 8–10 were used for qualitative comparison of local hydration products.

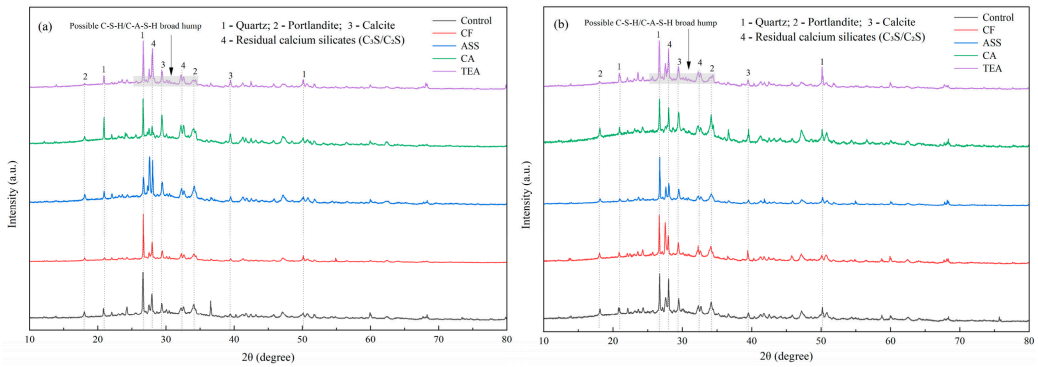


Figure 12. XRD patterns of RCP–GGBFS repair mortar with optimal dosages of different early-strength admixtures at 3 d and 28 d: (**a**) 3 d; (**b**) 28 d. The shaded region indicates the possible broad hump associated with poorly crystalline C-S-H/C-A-S-H gels. The XRD patterns were normalized and vertically shifted for clarity.

4. Discussion

The results show that the effectiveness of early-strength admixtures in RCP–GGBFS repair mortar depends not only on their accelerating effect, but also on their compatibility with the recycled binder system. Previous studies reported that calcium formate can promote hydration in fly ash–slag cementitious systems [27], sodium sulfate can enhance slag-containing binders through sulfate activation [39], calcium acetate can modify hydration and microstructure [28], and TEA has a dosage-dependent effect on cement hydration [56]. Compared with these studies, the originality of this work lies in comparing four different admixture chemistries under the same RCP–GGBFS polymer-modified repair mortar formulation while considering not only strength but also workability, tensile bond strength, drying shrinkage, SEM morphology, and XRD phase composition. From a practical perspective, the main risk is dosage sensitivity, especially the possible interfacial deterioration caused by excessive ASS and the strong dosage dependence of TEA. Because the GGBFS content in the present mixture was relatively low, the conclusions mainly reflect the compatibility of early-strength admixtures in a fixed polymer-modified repair mortar formulation investigated here, rather than in high-volume GGBFS systems. It should also be noted that tensile bond strength was evaluated only at 14 d in this study. Although the 3 d and 7 d flexural and compressive strengths were measured to characterize early strength development, the development of interfacial bond strength at 3 d and 7 d was not directly examined.

5. Conclusions

The effects of four early-strength admixtures on the workability, mechanical properties, tensile bond strength, drying shrinkage, and hydration characteristics of a P·I 42.5 cement-based repair mortar containing RCP and a low dosage of GGBFS were investigated. For the specific RCP–GGBFS repair mortar and dosage ranges considered in this work, the main conclusions are as follows:

1. All four early-strength admixtures exhibited dosage-dependent effects. The selected dosages were 1.5% CF, 1.0% ASS, 0.8% CA, and 0.05% TEA. At these dosages, the workability of the mortar was generally maintained, and the mechanical properties were improved to different degrees.
2. CF provided the most balanced performance. Compared with the control group, the 3 d and 28 d flexural strengths of the CF mixture increased by 37.0% and 20.3%, respectively. CF also showed relatively stable bond strength and shrinkage behavior, indicating good compatibility with the studied repair mortar system.
3. ASS produced the highest 14 d tensile bond strength. At 1.0% ASS, the tensile bond strength reached 1.052 MPa, which was 33.15% higher than that of the control group. However, its effective dosage range was narrow, and excessive ASS caused a sharp decrease in bond strength. This may be related to sulfate-induced crystallization pressure and microcrack development in the interfacial transition zone.
4. CA showed the most obvious shrinkage reduction in the present formulation. At 0.8% CA, the 28 d drying shrinkage decreased to 695.14×10^{-6}. This suggests that CA is more suitable when drying shrinkage control is prioritized. TEA mainly improved early compressive strength, with the 3 d compressive strength increasing by 39.4%, but its contribution to later-age compressive performance was limited.
5. SEM and XRD provided qualitative evidence that the early-strength admixtures mainly changed hydration development and local product morphology without generating new dominant crystalline phases. SEM observations showed different local distributions of AFt-like needle-shaped products, C-S-H gel, and CH among the mixtures, while XRD patterns mainly showed quartz, calcite, portlandite, and residual

calcium silicates. These microstructural results should be interpreted qualitatively because SEM observations were based on fractured surfaces, and XRD results may be affected by sampling representativeness.

6. For practical mixture selection in concrete structure and pavement repair, CF is preferable when balanced early strength, bond performance, workability, and dosage tolerance are required. ASS may be used for bond-strength-oriented repair, but its dosage should be strictly controlled because of its narrow effective range. CA is more suitable for shrinkage-sensitive repair mixtures, while TEA may be considered when early compressive strength improvement is the main requirement. These results provide practical guidance for selecting early-strength additives in low-carbon repair mortars and support the wider use of recycled concrete powder in repair materials for construction practice.

Author Contributions: Conceptualization, Y.G. and Q.L.; methodology, Y.G. and M.C.; validation, W.L. and Y.W.; formal analysis, W.L.; investigation, X.X.; resources, G.Y.; data curation, W.L. and Y.W.; writing—original draft preparation, Y.G. and W.L.; writing—review and editing, L.W.; visualization, W.L.; supervision, L.W. and M.C.; project administration, G.Y. and X.X.; funding acquisition, Q.L. All authors have read and agreed to the published version of the manuscript.

Funding: This research was funded by the National Natural Science Foundation of China [grant numbers 52478262]; the Qingdao Natural Science Foundation Youth Project [grant numbers 23-2-1-105-zyyd-jch]; and the Shandong Province City-Level School Enterprise Cooperation Project [grant numbers 2425282, 2425244, 2424360, 2423272].

Data Availability Statement: Data will be made available upon request.

Conflicts of Interest: The authors declare no conflicts of interest.

References

1. Yang, S.; Yang, D.; Shi, W.; Deng, C.; Chen, C.; Feng, S. Global evaluation of carbon neutrality and peak carbon dioxide emissions: Current challenges and future outlook. *Environ. Sci. Pollut. Res.* **2023**, *30*, 81725–81744. [CrossRef]
2. Zhou, N.; Price, L.; Yande, D.; Creyts, J.; Khanna, N.; Fridley, D.; Lu, H.; Feng, W.; Liu, X.; Hasanbeigi, A.; et al. A roadmap for China to peak carbon dioxide emissions and achieve a 20% share of non-fossil fuels in primary energy by 2030. *Appl. Energy* **2019**, *239*, 793–819. [CrossRef]
3. Liu, R.; Fang, Y.R.; Peng, S.; Benani, N.; Wu, X.; Chen, Y.; Wang, T.; Chai, Q.; Yang, P. Study on factors influencing carbon dioxide emissions and carbon peak heterogenous pathways in Chinese provinces. *J. Environ. Manag.* **2024**, *365*, 121667. [CrossRef] [PubMed]
4. Chou, J.; Li, Y.; Xu, Y.; Zhao, W.; Li, J.; Hao, Y. Carbon dioxide emission characteristics and peak trend analysis of countries along the Belt and Road. *Environ. Sci. Pollut. Res.* **2023**, *30*, 81881–81895. [CrossRef]
5. Schueremans, L.; Cizer, Ö.; Janssens, E.; Serré, G.; Van Balen, K. Characterization of repair mortars for the assessment of their compatibility in restoration projects: Research and practice. *Constr. Build. Mater.* **2011**, *25*, 4338–4350. [CrossRef]
6. Shi, J.; Liu, B.; Qin, J.; Jiang, J.; Wu, X.; Tan, J. Experimental study of performance of repair mortar: Evaluation of in-situ tests and correlation analysis. *J. Build. Eng.* **2020**, *31*, 101325. [CrossRef]
7. Ma, Q.; Geng, J.; Wei, P.; Xu, X.; He, Z.; Wang, Z.; Lan, H. Road performance of solid waste-based cementitious material-stabilized reclaimed base course material. *Materials* **2026**, *19*, 1462. [CrossRef] [PubMed]
8. Gao, Y.J.; Chen, J.L.; Li, Q.; Su, T.; Li, M.; Li, B.; Mei, X. Research progress on the preparation and performance of recycled mortars using solid waste-based cementitious materials. *Coatings* **2025**, *15*, 1483. [CrossRef]
9. Dung, N.T.; Chang, T.P.; Chen, C.T. Circulating fluidized bed combustion fly-ash-activated slag concrete as novel construction material. *ACI Mater. J.* **2015**, *112*, 105–114. [CrossRef]
10. Hou, X.; Li, J.; Guan, C.; Zhang, X.; Wang, X.; Li, Y.; Li, Y.; Shi, W.; Wang, W. Effect of carbonization on chloride penetration in rapid repair mortar derived from solid waste-based CSA cement. *Case Stud. Constr. Mater.* **2025**, *23*, e04956. [CrossRef]
11. Hou, X.; Li, J.; Xu, J.; Xiao, X.; Wang, J.; Liu, Y.; Ossman, M.; Lin, F.; Wang, X.; Li, Y.; et al. Experimental study of sulfoaluminate cement-based rapid repair mortar undergoing hot/wet harsh conditions: Mechanical strengths, hydration products, and ettringite evolution mechanism. *ACS Sustain. Chem. Eng.* **2024**, *12*, 10089–10101. [CrossRef]

12. Kaptan, K.; Cunha, S.; Aguiar, J. A review of the utilization of recycled powder from concrete waste as a cement partial replacement in cement-based materials: Fundamental properties and activation methods. *Appl. Sci.* **2024**, *14*, 9775. [CrossRef]
13. Song, R.; Yang, Q.; Song, H. Performance optimization and synergistic mechanism of ternary blended cementitious system composed of fly ash, slag, and recycled micro-powder. *Buildings* **2025**, *15*, 2780. [CrossRef]
14. Vaičiukynienė, D.; Liudvinavičiūtė, A.; Bistrickaitė, R.; Boiko, O.; Vaičiukynas, V. Alkali-activated slag repair mortar for old reinforced concrete structures based on ordinary Portland cement. *Materials* **2025**, *18*, 2272. [CrossRef] [PubMed]
15. Yahyaee, T.; Elize, H.S. A comprehensive study on mechanical properties, durability, and environmental impact of fiber-reinforced concrete incorporating ground granulated blast furnace slag. *Case Stud. Constr. Mater.* **2024**, *20*, e03190. [CrossRef]
16. Tadi, C.; Rao, T.C. Investigating the performance of self-compacting concrete pavement containing GGBS. *Mater. Today Proc.* **2022**, *49*, 2013–2018. [CrossRef]
17. Saluja, S.; Kaur, K.; Goyal, S.; Bhattacharjee, B. Long-term drying shrinkage of GGBFS-incorporated RCC under various temperature exposures. *J. Mater. Civ. Eng.* **2021**, *33*, 04021122. [CrossRef]
18. Murthy, A.R.; Prasanna, P.K.; Nipun, G.; Srinivasu, K.; Gandla, K.; Khan, A.H.; Sabi, E. Analysing the influence of ground granulated blast furnace slag and steel fibre on RC beams flexural behaviour. *Sci. Rep.* **2024**, *14*, 4914. [CrossRef] [PubMed]
19. Rawat, R.; Pasla, D. Assessment of mechanical and durability properties of FA-GGBS based lightweight geopolymer concrete. *Constr. Build. Mater.* **2024**, *426*, 135984. [CrossRef]
20. Singh, R.P.; Vanapalli, K.R.; Jadda, K.; Mohanty, B. Durability assessment of fly ash, GGBS, and silica fume based geopolymer concrete with recycled aggregates against acid and sulfate attack. *J. Build. Eng.* **2024**, *82*, 108354. [CrossRef]
21. Zhang, D.; Zhu, T.; Yang, Q.; Vandeginste, V.; Li, J. Influence of ground granulated blast furnace slag on recycled concrete powder-based geopolymer cured at ambient temperature: Rheology, mechanical properties, reaction kinetics and air-void characteristics. *Constr. Build. Mater.* **2024**, *438*, 137190. [CrossRef]
22. Wang, H.; Wang, L.; Shen, W.; Cao, K.; Sun, L.; Wang, P.; Cui, L. Compressive strength, hydration and pore structure of alkali-activated slag mortars integrating with recycled concrete powder as binders. *KSCE J. Civ. Eng.* **2022**, *26*, 795–805. [CrossRef]
23. Gopalakrishna, B.; Dinakar, P. Mix design development of fly ash-GGBS based recycled aggregate geopolymer concrete. *J. Build. Eng.* **2023**, *63*, 105551. [CrossRef]
24. Liu, M.; Wang, C.; Wu, H.; Yang, D.; Ma, Z. Reusing recycled powder as eco-friendly binder for sustainable GGBS-based geopolymer considering the effects of recycled powder type and replacement rate. *J. Clean. Prod.* **2022**, *364*, 132656. [CrossRef]
25. Tran, T.M.; Babalola, O.E.; Le, D.H. Experimental investigation of the performance of ground granulated blast furnace slag blended recycled aggregate concrete exposed to elevated temperatures. *Clean. Waste Syst.* **2023**, *4*, 100069. [CrossRef]
26. Shamass, R.; Rispoli, O.; Limbachiya, V.; Kovacs, R. Mechanical and GWP assessment of concrete using blast furnace slag, silica fume and recycled aggregate. *Case Stud. Constr. Mater.* **2023**, *18*, e02164. [CrossRef]
27. Wang, Y.; Jia, J.; Cao, Q.; Gao, X. Effect of calcium formate on the compressive strength, and hydration process of cement composite containing fly ash and slag. *J. Build. Eng.* **2022**, *50*, 104133. [CrossRef]
28. Lyu, B.-C.; Guo, L.-P.; Wu, J.-D.; Fei, X.-P.; Bian, R.-S. The impacts of calcium acetate on reaction process, mechanical strength and microstructure of ordinary Portland cement paste and alkali-activated cementitious paste. *Constr. Build. Mater.* **2022**, *359*, 129492. [CrossRef]
29. He, J.; Long, G.; Cong, M.; Xie, Y.; Shi, Y.; Li, N.; Cheng, Z. Effect of triethanolamine on hydration kinetics of cement–fly ash system at elevated curing temperature. *ACS Sustain. Chem. Eng.* **2020**, *8*, 10053–10064. [CrossRef]
30. Jia, J.; Wang, Y. Interactive effects of admixtures on the compressive strength development of Portland cement mortars. *Buildings* **2022**, *12*, 422. [CrossRef]
31. Wang, J.; Meng, T.; Chang, Z.; Tang, Y. Effect of different admixtures on the early strength of ternary all-solid waste geopolymer grouting materials. *Constr. Build. Mater.* **2026**, *525*, 146336. [CrossRef]
32. Cheng, X.Z.; Guo, T.D.; Cheng, Z.J.; Liu, L.; Li, C.H.; Luo, M.F.; Li, H.L.; Lv, R.; Cheng, Z. Synergistic effects of composite modifiers on mechanical properties and freeze-thaw durability of multi-solid waste cement mortar. *J. Build. Eng.* **2025**, *111*, 113299. [CrossRef]
33. Liu, C.; Yan, C.; Zhang, Y.; Wang, S. Preparation of early strength concrete using all solid waste-based cement: Strength formation mechanism and carbon footprint evaluation. *Constr. Build. Mater.* **2026**, *506*, 145071. [CrossRef]
34. George, M.; Sathyan, D. Life cycle assessment and structural evaluation of sustainable and cost effective engineered cementitious composite (ECC) repair mortars. *Front. Built Environ.* **2026**, *11*, 1721414. [CrossRef]
35. Li, J.W.; Xu, D.; Wang, X.J.; Wang, K.; Wang, W. Synergetic–complementary use of industrial solid wastes to prepare high-performance rapid repair mortar. *Front. Mater.* **2021**, *8*, 792299. [CrossRef]
36. Li, J.W.; Hou, X.S.; Jia, A.G.; Xiao, X.; Wang, X.J.; Yao, Y.G.; Zhang, Z.L.; Wang, W.L. Influencing factors and optimization on mechanical performance of solid waste-derived rapid repair mortar. *Waste Dispos. Sustain. Energy* **2023**, *5*, 223–234. [CrossRef]
37. Wu, X.; Li, B.; Wei, D.; Guo, F.; Ji, H. Investigation of preparation and shrinkage characteristics of multi-source solid waste-based cementitious materials. *Materials* **2023**, *16*, 7522. [CrossRef] [PubMed]

38. Wang, Y.; Lei, L.; Liu, J.; Ma, Y.; Liu, Y.; Xiao, Z.; Shi, C. Accelerators for normal concrete: A critical review on hydration, microstructure and properties of cement-based materials. *Cem. Concr. Compos.* **2022**, *134*, 104762. [CrossRef]
39. Fu, J.; Jones, A.M.; Bligh, M.W.; Holt, C.; Keyte, L.M.; Moghaddam, F.; Foster, S.J.; Waite, T.D. Mechanisms of enhancement in early hydration by sodium sulfate in a slag-cement blend—Insights from pore solution chemistry. *Cem. Concr. Res.* **2020**, *135*, 106110. [CrossRef]
40. Yang, S.; Wang, J.; Cui, S.; Liu, H.; Wang, X. Impact of four kinds of alkanolamines on hydration of steel slag-blended cementitious materials. *Constr. Build. Mater.* **2017**, *131*, 655–666. [CrossRef]
41. *GB 175-2023*; Common Portland Cement. Standards Press of China: Beijing, China, 2023.
42. *GB/T 18046-2017*; Ground Granulated Blast Furnace Slag Used for Cement, Mortar and Concrete. Standards Press of China: Beijing, China, 2017.
43. *JG/T 573-2020*; Recycled Fine Powder for Concrete and Mortar. Standards Press of China: Beijing, China, 2020.
44. *GB/T 25176-2010*; Recycled Fine Aggregate for Concrete and Mortar. Standards Press of China: Beijing, China, 2010.
45. *JC/T 2381-2016*; Repair Mortar. China Building Materials Industry Press: Beijing, China, 2016.
46. *GB/T 25181-2019*; Ready-Mixed Mortar. Standards Press of China: Beijing, China, 2019.
47. *GB/T 2419-2005*; Test Method for Fluidity of Cement Mortar. Standards Press of China: Beijing, China, 2005.
48. *GB/T 17671-2021*; Test Method of Cement Mortar Strength (ISO Method). Standards Press of China: Beijing, China, 2021.
49. *JGJ/T 70-2009*; Standard for Test Method of Basic Properties of Construction Mortar. China Architecture & Build-ing Press: Beijing, China, 2009.
50. Yamada, K.; Takahashi, T.; Hanehara, S.; Matsuhisa, M. Effects of the chemical structure on the properties of polycarboxylate-type superplasticizer. *Cem. Concr. Res.* **2000**, *30*, 197–207. [CrossRef]
51. Yamada, K.; Ogawa, S.; Hanehara, S. Controlling of the adsorption and dispersing force of polycarboxylate-type superplasticizer by sulfate ion concentration in aqueous phase. *Cem. Concr. Res.* **2001**, *31*, 375–383. [CrossRef]
52. Weng, T.-L.; Lin, W.-T.; Li, C.-H. Properties evaluation of repair mortars containing EVA and VA/VeoVa polymer powders. *Polym. Polym. Compos.* **2017**, *25*, 77–86. [CrossRef]
53. Gu, Y.; Dangla, P.; Martin, R.-P.; Omikrine Metalssi, O.; Fen-Chong, T. Modeling the sulfate attack induced expansion of cementitious materials based on interface-controlled crystal growth mechanisms. *Cem. Concr. Res.* **2022**, *152*, 106676. [CrossRef]
54. Li, Z.; Liu, J.; Xiao, J.; Zhong, P.; Wang, J. Drying shrinkage of mortar manufactured with recycled fine aggregate at vary initial saturation degree. *Constr. Build. Mater.* **2020**, *264*, 120621. [CrossRef]
55. Zou, F.; Hu, C.; Wang, F.; Ruan, Y.; Hu, S. Enhancement of early-age strength of the high content fly ash blended cement paste by sodium sulfate and C–S–H seeds towards a greener binder. *J. Clean. Prod.* **2020**, *244*, 118566. [CrossRef]
56. Lu, Z.; Kong, X.; Jansen, D.; Zhang, C.; Wang, J.; Pang, X.; Yin, J. Towards a further understanding of cement hydration in the presence of triethanolamine. *Cem. Concr. Res.* **2020**, *132*, 106041. [CrossRef]

Disclaimer/Publisher's Note: The statements, opinions and data contained in all publications are solely those of the individual author(s) and contributor(s) and not of MDPI and/or the editor(s). MDPI and/or the editor(s) disclaim responsibility for any injury to people or property resulting from any ideas, methods, instructions or products referred to in the content.